Smart Structures and Systems, *Vol. 23, No. 2 (2019) 123-139*
DOI: https://doi.org/10.12989/sss.2019.23.2.123

Impact force localization for civil infrastructure using augmented Kalman Filter optimization

Muhammad M. Saleem[1,2a] and Hongki Jo[*1]

[1]*Department of Civil Engineering and Engineering Mechanics, The University of Arizona, 1209 E 2nd street Tucson, AZ 85719, USA*
[2]*Department of Civil Engineering, University of Engineering and Technology Lahore, G.T. Road Lahore, 54890, Pakistan*

(Received January 1, 2018, Revised December 23, 2018, Accepted January 16, 2019)

Abstract. Impact forces induced by external object collisions can cause serious damages to civil engineering structures. While accurate and prompt identification of such impact forces is a critical task in structural health monitoring, it is not readily feasible for civil structures because the force measurement is extremely challenging and the force location is unpredictable for full-scale field structures. This study proposes a novel approach for identification of impact force including its location and time history using a small number of multi-metric observations. The method combines an augmented Kalman filter (AKF) and Genetic algorithm for accurate identification of impact force. The location of impact force is statistically determined in the way to minimize the AKF response estimate error at measured locations and then time history of the impact force is accurately constructed by optimizing the error co-variances of AKF using Genetic algorithm. The efficacy of proposed approach is numerically demonstrated using a truss and a plate model considering the presence of modelling error and measurement noises.

Keywords: augmented Kalman filter; genetic algorithm; strain gauges; accelerometers; impact force

1. Introduction

Civil engineering structures are subjected to different types of dynamic loadings including earthquake load, wind load, traffic load and accidental collision load etc. The identification of these loads is important for the design and monitoring of these structures. Direct measurement of these loads using load transducers is not actually feasible primarily because their exact locations are not known in most of the cases. Sometimes the loads are distributed over so many locations that the use of load transducers does not remain practical. That is why many indirect methods have been proposed for the estimation of applied loads using measured structural response. (Liu *et al*. 2000, Ma and Dong 2000, Qiu and Shenfang 2011).

As a type of dynamic loads, an impact load is a high force of one or more objects striking against another and applied over short time period. Because an impact force is generally applied to small contact area of the colliding objects with significant energy, it has greater effects than distributed loads applied over longer period. If such impact loads are neither expected, nor considered in the structural designs, the structures will be exposed to unforeseeable structural risk.

Particularly, many accidents of vehicle collisions with bridges have been reported in the past and some have even resulted in the collapse of the bridge (Buth *et al.* 2010). For instance, on May 19, 1993 a tractor with semitrailer driving on I-65 near Evergreen, Alabama hit a bridge pier of the County Road 22 overpass and resulted in the collapse of two bridge spans. Later, two other vehicles collided with the collapsed bridge killing both the drivers. A similar accident occurred on I-45 in Texas on September 9, 2002 when a tractor-trailer hit bridge column of Highway 14 overpass, collapsing the bridge and killing one person. Another bridge collapse due vehicular collision occurred on May 23, 2003 when a semitrailer crashed into the support of bridge crossing I-80 near Big Springs Nebraska (El-tawil *et al.* 2005). Prompt identification of such collision events enables timely decisions to be made regarding the structure use restrictions to preemptively avoid yet another consequential catastrophe. In addition, accurate identification of the magnitude time histories and applied location of the collision-induced impact force can provide essential information for understanding the impact-induced structural behaviors.

A number of studies have been conducted for identifying the impact force over the last decades, mostly for aircraft composite panels. Most straightforward approach is to use trigonometric location techniques (Staszewski *et al*. 2009, Mahzan 2007). In triangulation, stress waves generated due to impact event are recorded by, at least, three sensors simultaneously and then impact location is determined by considering wave velocities and traveling times in the medium. But this approach is not readily feasible for relatively complex and composite structures, because the wave velocities are highly dependent on the properties of wave propagation paths (Meo *et al.*

*Corresponding author, Assistant Professor
E-mail: hjo@email.arizona.edu
[a] Ph.D. Student

ISSN: 1738-1584 (Print), 1738-1991 (Online)

2005). Optimized sensor triangulation has been proposed, which combines classical triangulation with Genetic algorithm (Coverley and Staszewski 2003). Improved results have been observed with this method for composite panels. However, these wave-based approaches still have limitation in applying for large systems where wave energies are not sufficient to cover the whole structures, but is more suitable for local identification.

Machine learning-based techniques have been introduced for impact force identification (Worden and Staszewski 2000, Sharif *et al.* 2012, LeClerc *et al.* 2007, Sung *et al.* 2000). For instance, a neural network in combination with Genetic algorithm has been studied to identify impact force using dynamic strain measurements (Worden and Staszewski 2000). Sharif *et al.* (2012) used artificial neural network to identify a large number of impacts over a wide range of energies at different locations of a composite plate. LeClerc *et al.* (2007) applied regression, identification and their combination to neural network for impact force identification on an aircraft composite panel. Sung *et al.* (2000) detected the impact location using acoustic signal information in neural network paradigms. Mahzan *et al.* (2010) compared the modified triangulation method with Artificial Neural Network for impact damage detection in composite aerospace structures. Machine learning approaches have exhibited good ability to handle complex problems but the requirement of large training test data is a critical hurdle of these methods in applying for real systems (Yan *et al.* 2017).

Another approach for impact force identification is based upon system modelling. In these methods, dynamic structural responses, generated by numerical models subjected to impact forces, are compared with sensor measurements (Staszewski *et al*. 2009). For example, Choi and Chang (1996) used a smoother algorithm on distributed piezoelectric sensor measurements for a simple Bernolli-Euler Beam model to identify impact load. Saydel and Chang (2001) modified the model proposed by Choi and Chang (1996) to detect low velocity impacts on stiffened composite panels. Yan and Zhou (2009) proposed a genetic algorithm based approach for impact force identification. They represented impact force as a set of parameters and then used genetic algorithm to estimate those parameters by minimizing the difference between estimated and measured dynamic response. Zhang *et al.* (2014) monitored low velocity impact on a CFRP composite plate using a model reconstruction algorithm based on support vector regression. The model-based methods have also been developed based on deconvolution of inverse analysis. (Inoue *et al.* 2001). For instance, frequency response function (FRF) matrix and response measurements can be used to estimate the input excitations. But the inversion of FRF, involved in the process, is an ill-posed problem and may suffer from un-stability in case of noise. (Guillaume *et al.* 2002, Ma *et al.* 1998). Such ill-posed issues of inverse problems can be improved by employing regularization techniques (Jacquelin *et al*. 2003, Busby and Trujillo 1997, Hansen 1992). Yun *et al.* (2017) employed Bayesian regularization to obtain stable identification of the impact forces for composite plates. However, these regularization methods have been known to be computationally inefficient for large size of formulated linear problems (Golub and Urs 1997).

Lourens *et al.* (2012) introduced an augmented Kalman filter for input force identification in which input force is estimated by incorporating input forces as part of state vector and applied for a simple beam structure. However, incorporation of input force in the state vector may intrinsically suffer from instability issue when acceleration measurements are only used in the measurement update process. Naets *et al*. (2015) improved the instability issue of the augmented Kalman filter by employing dummy displacement measurements. Khodabandeloo and Jo (2015) utilized multi-metric measurements to address the instability issue as well as improve the accuracy of the augmented Kalman filter. However, these augmented Kalman filter based methods have been validated only for the cases where input force locations were known.

This paper presents a novel approach for simultaneous identification of impact force location and its time history by combining augmented Kalman filter with Genetic algorithm. Proposed method uses small numbers of multi-metric measurements. The impact force location is statistically identified in the way to minimize response estimation errors at the measured locations. Impact force time history is then accurately reconstructed by optimizing the error co-variances of the Kalman filter for the identified impact location. Possible uncertainties in numerical modeling and measurements are effectively considered through the Kalman filter process, making it more feasible for practical applications. The rest of this paper is structured as follows. Section 2 describes the state space model used for numerical simulations and the augmented Kalman filter formulation. Section 3 explains the detail of the proposed methodology for impact force identification. Numerical examples are presented to demonstrate the effectiveness of the proposed method in section 4. Finally, conclusions are drawn in section 5.

2. Problem formulation

The proposed method combines augmented Kalman filter(AKF) and Genetic algorithm(GA) to locate the applied impact force and reconstruct its time history by optimizing the error co-variance matrices.

2.1 State space model

The dynamic behavior of a linear system is described by Eq. (1)

$$\mathrm{M\ddot{u}(t) + C\dot{u}(t) + Ku(t) = S_p f(t)} \quad (1)$$

Where M, C, K, and f are mass, damping, stiffness, and force matrices respectively. M, C, and K are 'n x n' matrices with 'n' being the total number of degrees of freedom. S_p is 'n x n_p' force selection matrix, where n_p is the number of degrees of freedom which forces are acting at. The continuous state space formulation of Eq. (1) can be expressed as (Juang and Phan 2001)

$$\dot{x}(t) = A_c x(t) + B_c f(t)) \tag{2}$$

Where

$$x(t) = \begin{Bmatrix} u(t) \\ \dot{u}(t) \end{Bmatrix};\ A_c = \begin{bmatrix} 0 & I \\ -M^{-1}K & -M^{-1}C \end{bmatrix}$$
$$B_c = \begin{bmatrix} 0 \\ M^{-1}S_p \end{bmatrix} \tag{3}$$

In the above equations 'x' is the state vector composed of structural displacement and velocity responses. Eq. (4) expresses the measurements in terms of the states of the system

$$y(t) = G_c x(t) + D_c f(t) \tag{4}$$

The state Eq. (2) and measurement Eq. (4) constitute state space model of the system in continuous form. The discrete time form of the state space model can be defined as

$$x_{k+1} = Ax_k + Bf_k \tag{5}$$

$$y_k = Gx_k + Df_k \tag{6}$$

Where

$$A = e^{A_c \Delta t} \quad ; \quad B = (A - I){A_c}^{-1}B_c$$
$$G = G_c;\ D = D_c \tag{7}$$

The Kalman Filter estimates the system states using state space model while considering possible model error (m_k) and measurement noise (z_k), so Eqs. (5) and (6) become

$$x_{k+1} = Ax_k + Bf_k + m_k \tag{8}$$

$$y_k = Gx_k + Df_k + z_k \tag{9}$$

2.2 Kalman filter

Kalman filter (KF) is an algorithm that estimates linear states in a statistically optimal manner when provided with measurements having uncertainties. The KF uses system model to predict the states (i.e., structural responses) and update the prediction using observations. Its modified form that can be used for the prediction of both structural responses and applied forces is known as augmented Kalman filter (AKF) (Lourens *et al.* 2012). This research uses the AKF for identifying unknown impact forces.

Kalman filter has two main steps, i.e., measurement update and time update (Bishop and Welch 2001).

Measurement update

$$K_k = P_k^- G^T (GP_k^- G^T + F)^{-1}$$
$$\hat{x}_k = \hat{x}_k^- + K_k(y_k - G\hat{x}_k^-) \tag{10}$$
$$P_k = (I - K_k G)P_k^-$$

Time update

$$\hat{x}_k^- = A\hat{x}_{k-1}^- + Bf_{k-1}$$
$$P_k^- = AP_{k-1}^- A^T + E \tag{11}$$

Where P_k^- and P_k are a priori and a posteriori estimate error co-variances respectively. E and F are modelling error and measurement noise co-variance matrices respectively and their order of magnitude is determined by the state vector magnitude order and signal to noise ratio (Lourens *et al.* 2012). For more details on these terms see Bishop and Welch (2001).

2.3 Augmented Kalman filter (AKF)

Conventional KF approach can estimate the structural response if the excitation force is known. However, the applied force is not known in practical problems most of the times. The augmented Kalman filter (AKF), an updated form of traditional Kalman filter, is employed in this research to address this problem of unknown force excitations. In this approach, input force is made a part of state vector (i.e., augmented state vector) and is estimated with the structural response. Random walk model is employed to incorporate the force term into existing state vector, its formulation in the continuous domain is given as

$$\dot{f} = 0 + \beta \tag{12}$$

Where β is the force model noise on the derivative of force parameter, meaning that force increment is a totally random process. Its discrete version is expressed as

$$f_{k+1} = f_k + \beta_k \tag{13}$$

Then the augmented form of the state vector obtained by including input force is

$$\begin{Bmatrix} \dot{x}(t) \\ \dot{f}(t) \end{Bmatrix} = \begin{bmatrix} A_c & B_c \\ 0 & 0 \end{bmatrix} \begin{Bmatrix} x(t) \\ f(t) \end{Bmatrix} + \begin{Bmatrix} m \\ \beta \end{Bmatrix} \tag{14}$$

$$A_{ac} = \begin{bmatrix} A_c & B_c \\ 0 & 0 \end{bmatrix};\ \zeta = \begin{Bmatrix} m \\ \beta \end{Bmatrix} \tag{15}$$

Where A_{ac} is the continuous form of system matrix in augmented formulation and ζ is the noise vector.

Observation equation takes the form

$$y = G_{ac} \begin{Bmatrix} x(t) \\ f(t) \end{Bmatrix} + z \tag{16}$$

$$G_{ac} = [G \quad D] \tag{17}$$

The augmented state vector and state equation in discrete form are

$$X_k^a = \begin{Bmatrix} X_k \\ f_k \end{Bmatrix}_{(n_s + n_p) \times 1} \tag{18}$$

Where 'n_s' is the number of states

$$X_{k+1}^a = A_a X_k^a + \zeta_k \tag{19}$$

$$A_a = \begin{bmatrix} A & B \\ 0 & I \end{bmatrix} \tag{20}$$

The observation equation becomes

$$y_k = G_a X_k^a + z_k \tag{21}$$

$$G_a = [G \quad D] \tag{22}$$

Matrices *G* and *D* are given in Eq. (30)

So, the time and measurement update equations for AKF method becomes (Lourens *et al.* 2012);

Measurement update

$$\begin{aligned} L_k &= P_{k|k-1} G_a^T (G_a P_{k|k-1} G_a^T + F)^{-1} \\ \hat{X}_{k|k}^a &= \hat{x}_{k|k-1}^a + L_k\left(y_k - G_a \hat{x}_{k|k-1}^a\right) \\ P_{k|k} &= P_{k|k-1} - L_k G_a P_{k|k-1} \end{aligned} \tag{23}$$

Time update

$$\begin{aligned} \hat{X}_{k+1|k}^a &= A_a \hat{X}_{k|k}^a \\ P_{k+1|k} &= A_a P_{k|k} A_a^T + E_a \end{aligned} \tag{24}$$

In AKF formulation, augmented co-variance matrix 'E_a' is formed by combining the modelling error co-variance matrix '*E*' with regularization matrix '*H*'

$$E_a = \begin{bmatrix} E & 0 \\ 0 & H \end{bmatrix} \tag{25}$$

The relationship between measurements and structural response used in the measurement matrix G_a of augmented state space form can be expressed as

$$y(t) = S_a \ddot{u}(t) + S_v \dot{u}(t) + S_d u(t) \tag{26}$$

Where S_a, S_v, and S_d are '$n_m \times n$' selection matrices corresponding to acceleration, velocity, and displacement respectively. 'n_m' is the number of measurements and 'n' is the number of degree of freedoms.

Putting the expression of $\ddot{u}(t)$ from Eq. (1) to Eq. (26) and rearranging them, we get

$$\begin{aligned} y(t) = (S_v - S_a M^{-1} C)\dot{u}(t) + (S_d - S_a M^{-1} K) u(t) \\ + S_a M^{-1} S_p f(t) \end{aligned} \tag{27}$$

So

$$\begin{aligned} G = G_c = [S_d - S_a M^{-1} K \ , \ \ S_v - S_a M^{-1} C \,] \\ D = D_c = S_a M^{-1} S_p \end{aligned} \tag{28}$$

If observations include strain measurements then strains can be expressed as the linear combinations of displacement states, so Eq. (26) becomes

$$y(t) = S_a \ddot{u}(t) + S_v \dot{u}(t) + S_d u(t) + S_s u(t) \tag{29}$$

Where S_s is the strain selection matrix. So, if strain measurements are considered, Eq. (28) becomes

$$\begin{aligned} G = G_c = [S_s + S_d - S_a M^{-1} K \ , \ \ S_v - S_a M^{-1} C \,] \\ D = D_c = S_a M^{-1} S_p \end{aligned} \tag{30}$$

3. Proposed impact force localization method

Two sets of sensor measurements, i.e., structural responses, are used in conjunction with augmented Kalman filtering process for the proposed model-based impact force localization. Once the sensors are placed on the structure, structural response measurements from a portion of the sensors (hereafter called SE-sensors) are used for state estimation in the Kalman filtering process with the initially assumed location of applied impact force and assumed error covariance values. And measurements from the remaining sensors (hereafter called AD-sensors) are utilized as references to compare them with estimated responses from the Kalman filtering process. This process is repeated for all potential locations of the impact force and the root mean square (RMS) estimation errors between measured and estimated responses at the AD-sensor locations are calculated using the Eq. (31). The minimum-error location would be the tentative impact force location.

$$\text{RMS Error} = \sqrt{\frac{\sum(\varepsilon_{est} - \varepsilon_{mea})^2}{\text{Signal length}}} \tag{31}$$

Sensors may be placed at the maximum expected response locations based upon engineering judgement or in further optimized ways. Once the sensors are installed, their positions remain fixed; however, their roles can switch from SE-sensors to AD-sensors and vice versa. The tentative impact force locations are estimated again for all other different combinations of SE- and AD-sensor roles. Then the final impact force location is statistically determined considering all those combinations; which may have the minimum mean value and standard deviation for the average estimation errors.

Once the impact force is located, then Genetic Algorithm (GA) is applied to decide the optimized covariance values in a way to further minimize the average estimation error at the AD sensor locations. The error covariance values obtained from GA are then used in the augmented Kalman filtering process to reconstruct the accurate time history of the impact force.

In order to improve the stability of the Kalman filtering process and estimation accuracy, two types of multimeric sensors, i.e. strain gauges and accelerometers, are used in this research. Acceleration-only-based augmented Kalman filtering process may cause un-stability issue when modeling errors and/or measurement noises are considered (Naets *et al.* 2015, Khodabandeloo and Jo 2015). And accuracy improvement of many structural monitoring methods over broad frequency range by using multi-metric measures has been demonstrated (Khodabandeloo and Jo, 2015, Sim *et al.* 2011, Kijewski *et al.* 2006). Fig. 1 shows the flow chart of the proposed algorithm.

4. Numerical examples

Two numerical examples, a truss bridge and a cantilever plate, have been considered to validate the proposed approach for impact force identification. Finite element models of both structures have been developed in Matlab considering possible uncertainties in modeling (inbuilt 5% model error). Materials properties are set same as A-36 steel.

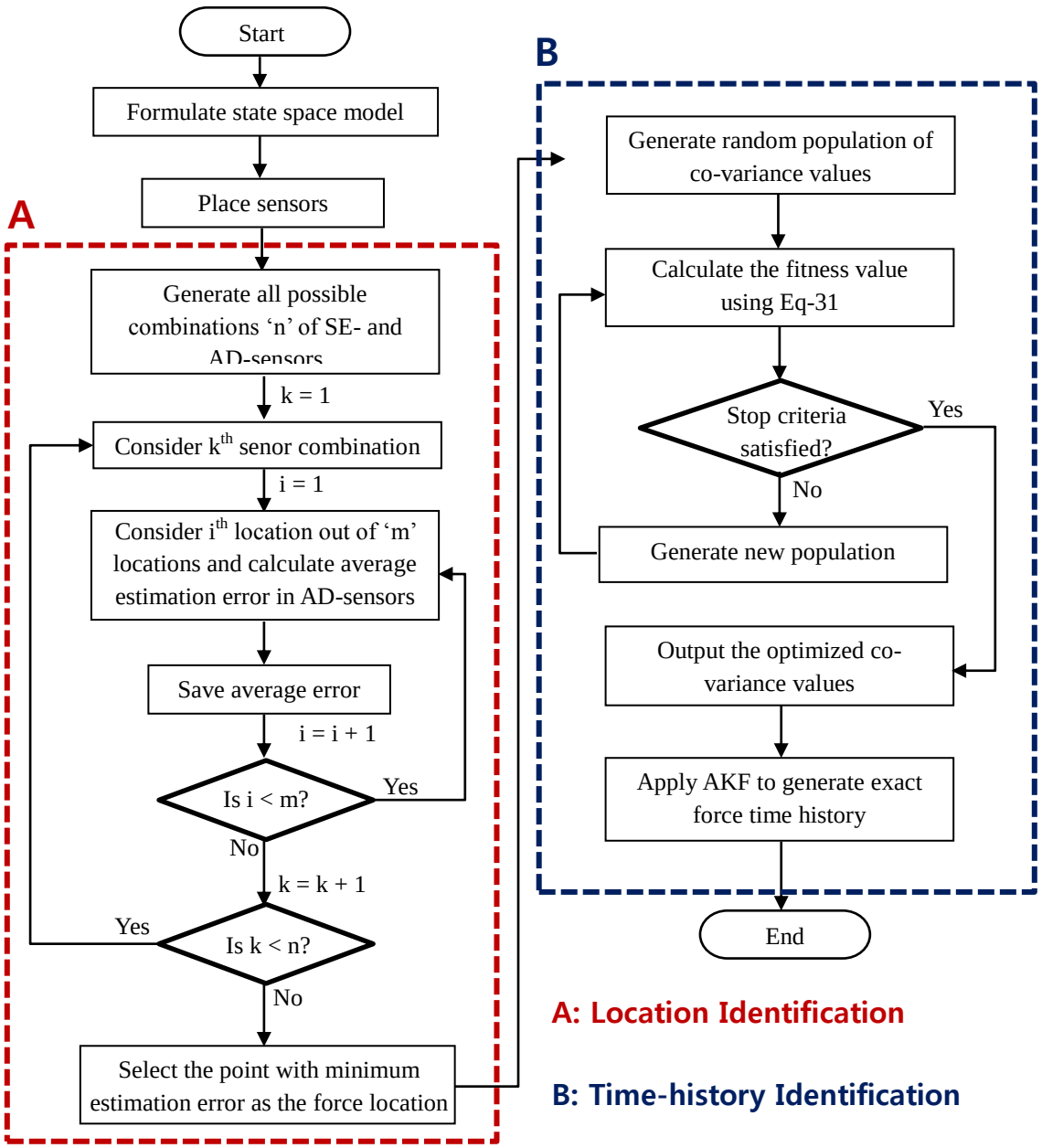

Fig. 1 Flow Chart of the proposed impact force localization algorithm

An impact force combined with random noise is applied on both structures. Time histories of the structural responses have been generated by using Matlab SIMULINK.

Two types of measurement noises, i.e., absolute and relative, are considered in all the simulations. Absolute measurement noise is closer to the many of commercially available sensor specification; 1μ-strain and 1mg are added in strain and acceleration responses respectively (Khodabandeloo *et al.* 2017). Relative noise is also considered to account for possible sources of additional noises due to harsh environment, long cabling, and improper setup; 10% relative noise is added to each measurement.

4.1 Truss structure

A simply supported 9-bay truss with 34-members and 18 joints is modelled. The geometry of the truss is shown in Fig. 2. Cross-sectional areas of the truss members are given in Table 1. The Impact force is applied at the node no. 14 in vertical direction. Two different cases of sensor combination are considered for impact force identification.

Case-1: strain gauges as AD-sensors.

Case-2: Accelerometers as AD-sensors.

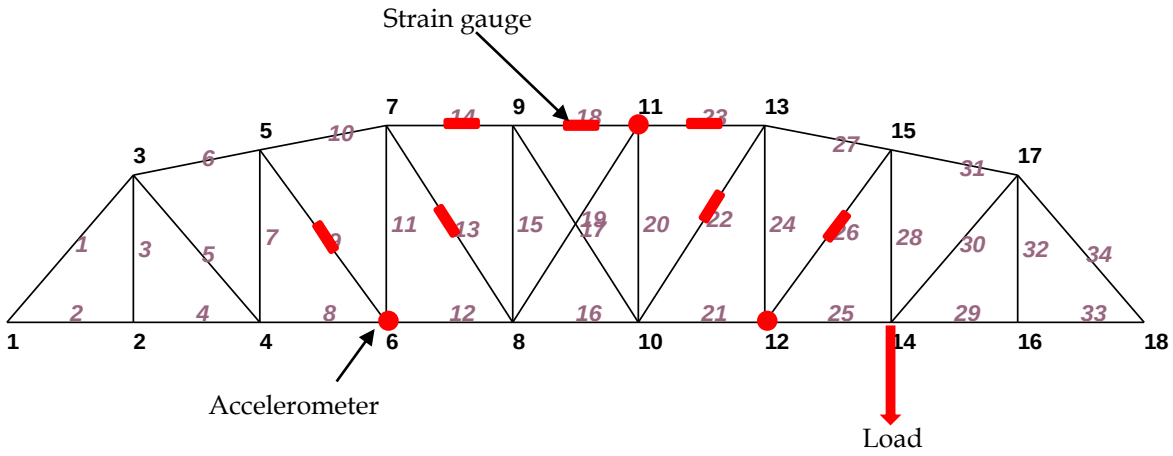

Fig. 2 Truss geometry and Multi-metric sensor arrangement for Case-1 simulation

Table 1 Cross-sectional areas of truss members

Element No.	Sectional area (cm^2)
1, 6, 10, 14, 18, 23, 27, 31, 34	15
2, 3, 4, 7, 8, 11, 12, 15, 16, 20, 21, 24, 25, 28, 29, 32, 33	9.75
5, 9, 13, 17, 19, 22, 26, 30	4.75

4.1.1 Case-1: Strain measurement for AD-sensor data

Total ten sensors, i.e., seven strain gauges and three accelerometers, are installed on the truss as shown in Fig. 2. These accelerometers measure acceleration responses in vertical direction and will be used as SE-sensors for the Kalman filtering process. Three of the strain gauges are also used as SE-sensors and remaining four strain gauges are used as AD-sensors. Total thirty-five unique combinations can be generated by considering three out of seven strain gauges as SE-sensors and remaining as AD-sensors. All of these sensor role combinations are considered for the analysis. For every combination, the impact force is assumed to be acting at a node from 2 to 17 one by one to find the minimum estimation error location.

Example results for the state (i.e., impact force and structural responses) estimation for one of the sensor role combinations with initially assumed (incorrect) impact force location and assumed co-variances are shown in Fig. 3. Strain gauges at the members 9, 13, 14, and 22 are used as the AD-sensors in this particular combination. As shown in Fig. 3(a), the impact force estimate is absolutely incorrect and strain response estimates (Figs. 3(b) and 3(c)) have large errors. About 10kN impact force has been applied 0.98 second later since low-level random excitation has been provided. However, estimated strain response at member #9 (one of the AD sensor locations) did not catch the expected impulse response around 1 second (Fig. 3(b)), showing 6.18 μ-strain RMS error for that member. Strain estimation errors for entire truss members are shown in Fig. 3(c), average RMS error for all the members is 3.18 μ-strain for this particular sensor role combination.

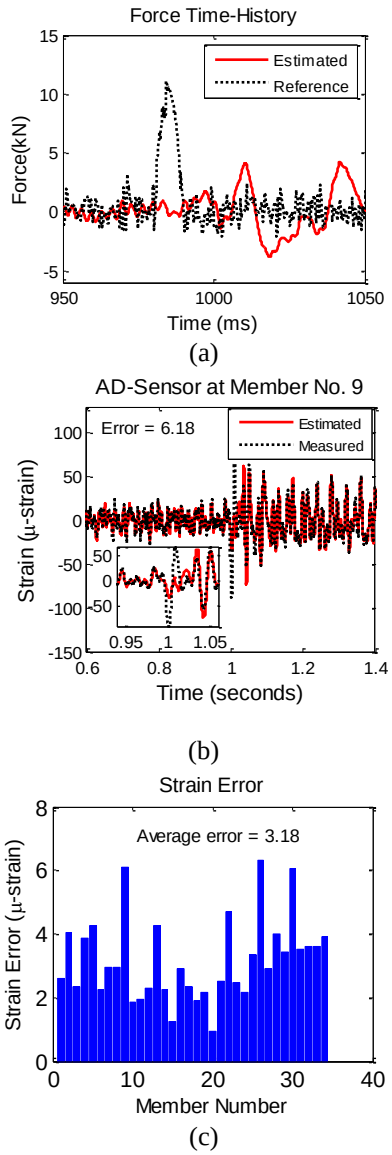

Fig. 3 Example of (a) impact force and (b) and (c) strain response estimations with incorrect force locati on and assumed co-variance values

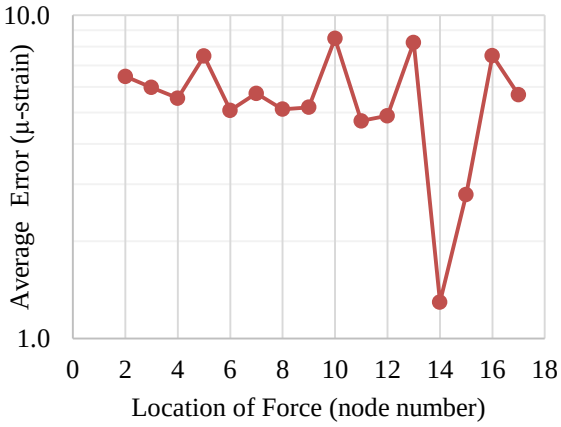

Fig. 4 Variation in average strain error at AD-sensor locations with changing force location

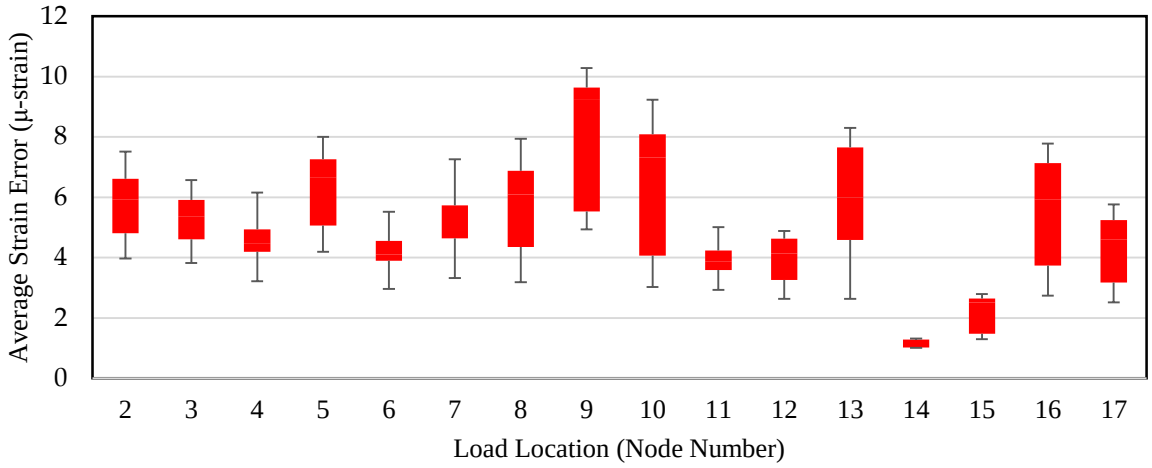

Fig. 5 Distribution of average strain error with change in force location for all sensor role combinations

Average strain estimation error in AD-sensor location has been calculated for all the sensor role combinations and possible impact force locations. The variation in the average strain error with the assumed location of impact force is shown in Fig. 4 for one of the sensor role combinations.

As shown in Fig. 4, the average strain error is the smallest when the assumed force location coincides the actual location which is node 14 in this example. Similar patterns have been observed for all the thirty-five sensor role combinations. The distribution of average error for all the combinations is shown in Fig. 5. Both the mean value of average strain error and its variation are the smallest at the node-14, indicating the node-14 is the most probable location of the applied impact force.

Optimized Covariance Matrix for Kalman Filter

Optimized covariance matrix for the AKF process can significantly improve the accuracy of estimated impact force. Assumed co-variance values are temporarily used for the beginning to locate the impact force. Once the most probable location of the impact force is identified, then Genetic Algorithm (GA) is applied to optimize the co-variance values in the way to minimize the average strain-estimation error in AD-sensors. The optimized co-variance values are then used in AKF again to get the more accurate time-history of the impact force and structural responses for the structure.

The comparison of the impact force time-history with optimized and un-optimized error co-variances is given in Fig. 6. Substantial improvement can be observed for the accuracy of estimated impact force time history.

However, the efficacy of the covariance matrix optimization for structural response estimations is not as significant as it is for impact force estimation. The comparison of strain errors in all truss members between estimated and actual strain responses for optimized and un-optimized co-variance values is presented in Fig. 8.

As shown in the Fig. 8, the accuracy of the structural response estimation can be somewhat improved by optimizing the covariance matrices; average strain estimation error for all members is reduced from 0.174 to 0.141 μstrain. However, the estimated strain responses even with un-optimized (initial) covariance matrix, but for correct impact location, are still acceptable except the

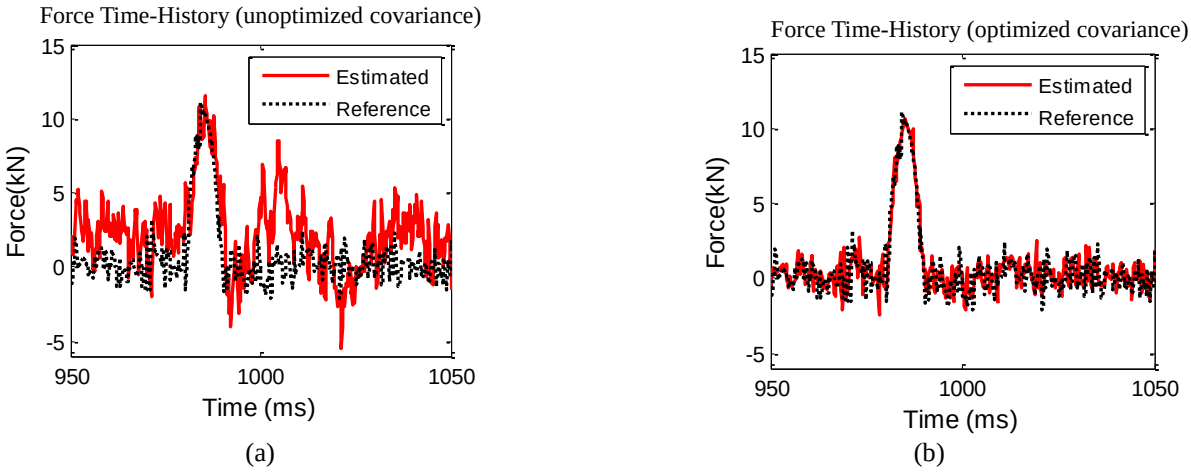

Fig. 6 Comparison of Force Time-History with (a) unoptimized and (b) optimized co-variance values

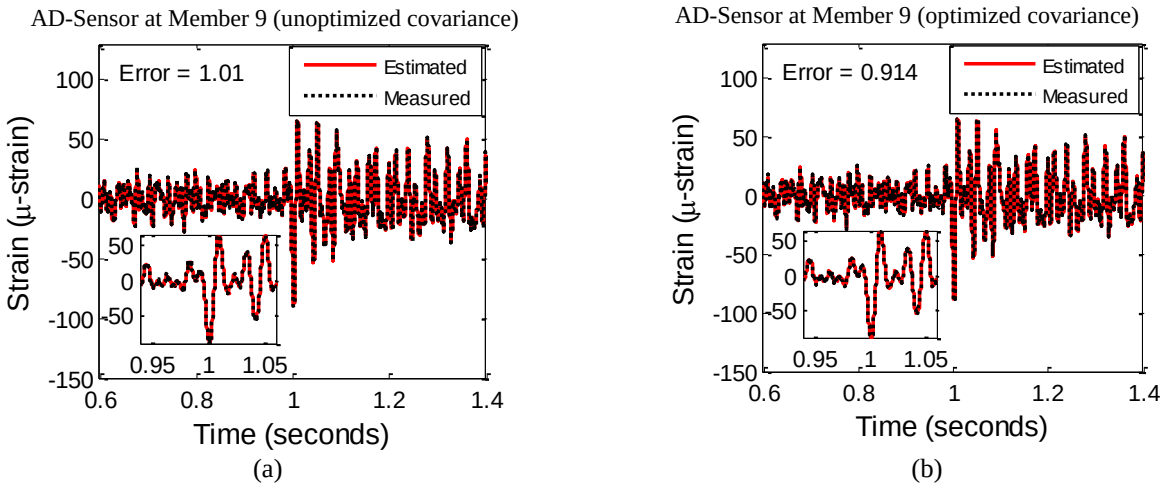

Fig. 7 Comparison of estimated and measured strain time-histories of an AD-sensor for (a) unoptimized and (b) optimized co-variance values

estimations for a few of members (e.g., member #25, 26, 28, 29, 30). Similar observation can be made from Fig. 7, which shows an example comparison of measured and estimated strain time histories for one of AD-sensor locations, i.e., at member 9, for optimized vs. un-optimized co-variance values. This less effect of co-variance optimization on the response estimation may be attributed to a better initial guess of the co-variance values.

As long as the impact force location is correctly identified, the general quality of structural response estimation is not so sensitive to the optimization of the covariance matrix. Comparison of the Fig. 6 (with correct location of the impact force) with the Fig. 3 (with incorrect location) reveals that how critical the correct localization of the applied forces is for the model-based state estimation of dynamic structures. Figs. 6-8 show that the impact force and structural response can be well estimated using the proposed method. It is noteworthy that all the simulations are carried out on Intel(R) Xeon(R) CPU E5-2630 v3 @ 2.40GHz with 32GB RAM and each impact force identification takes about 20 minutes for this specific numerical example.

Results with 10% measurement noise

The effect of relative measurement noise on the quality of force and response estimation of the structure is also studied. 10% measurement noise is added in all the sensor measurements. Both the impact force and structural response are successfully identified with this noise level. Example results of force and structural response estimates for 10% measurement noise are presented in Fig. 9.

4.1.2 Case-2: Acceleration measurements for AD-sensor data

The case using accelerometers as the AD-sensors has been investigated. Total number of sensors, i.e., 10, are the same as the case 1 above. But more accelerometers are used for the same truss structure, i.e. seven accelerometers and

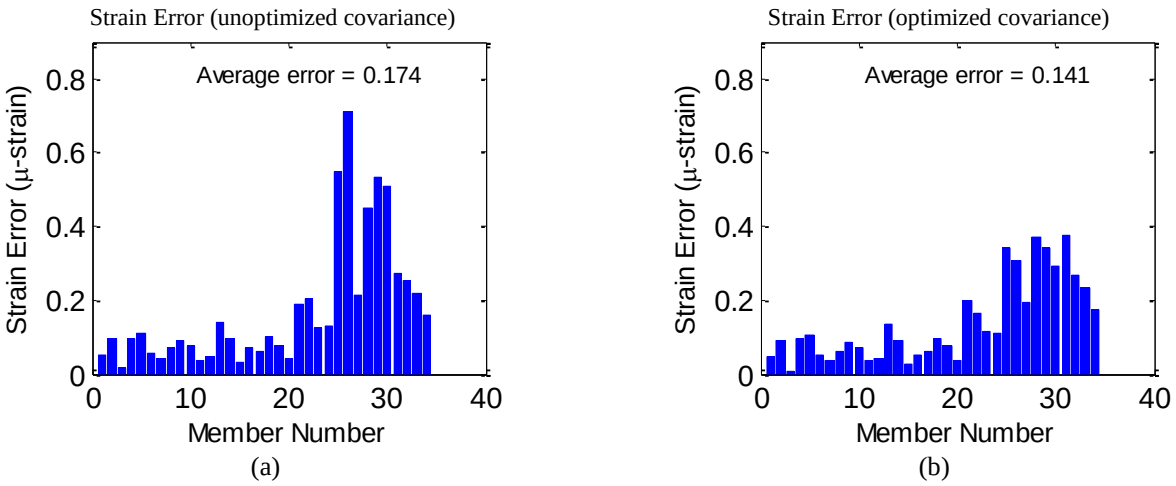

Fig. 8 Comparison of member strain errors between actual and estimated strain with (a) unoptimized and (b) optimized co-variance values

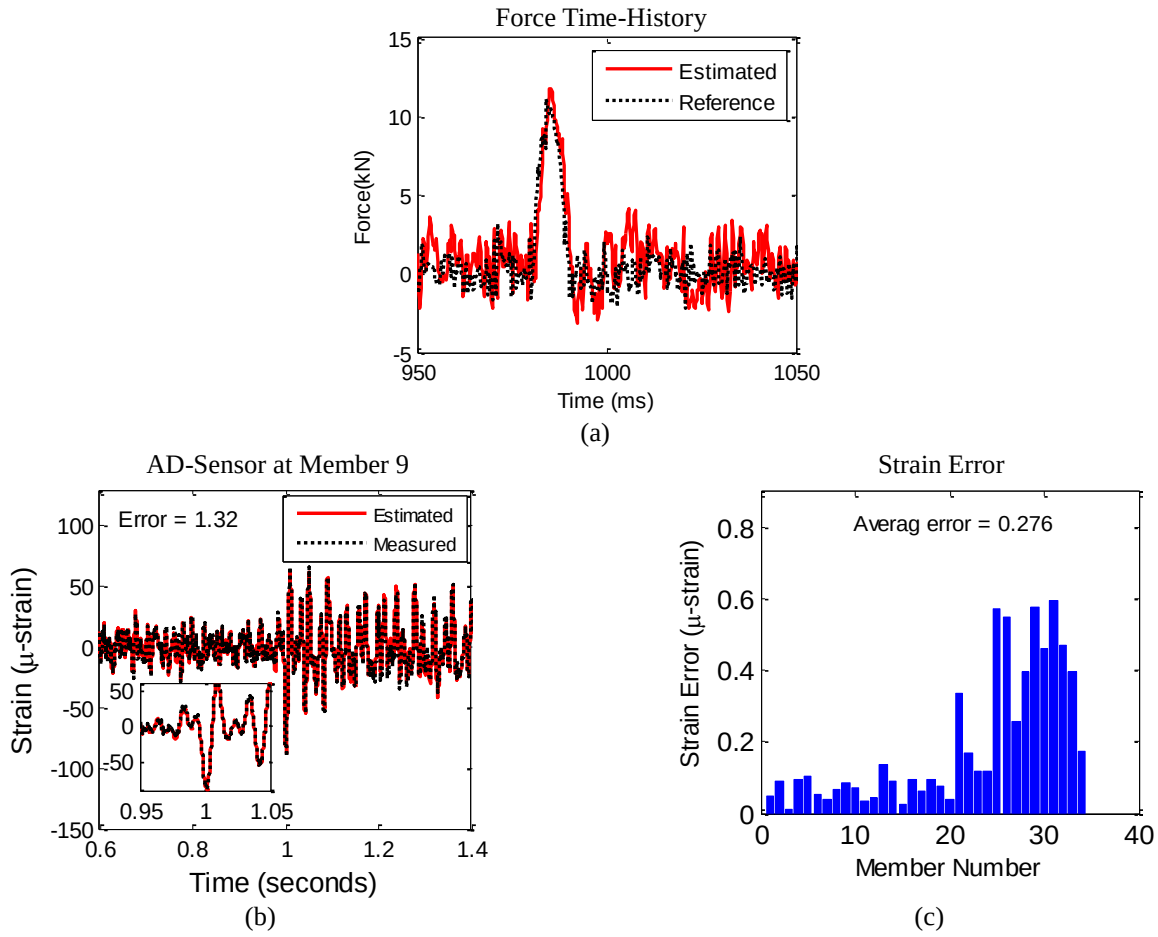

Fig. 9(a) Impact force and (b) and (c) strain response estimations with correct force location and optimized co-variance values considering 10% measurement noise

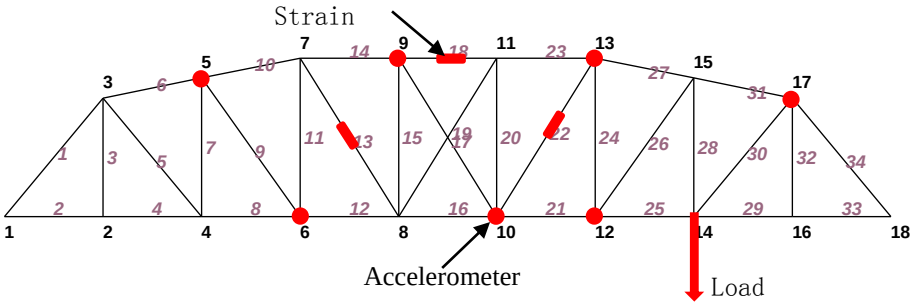

Fig. 10 Multi-metric sensor arrangement for Case-2 simulation

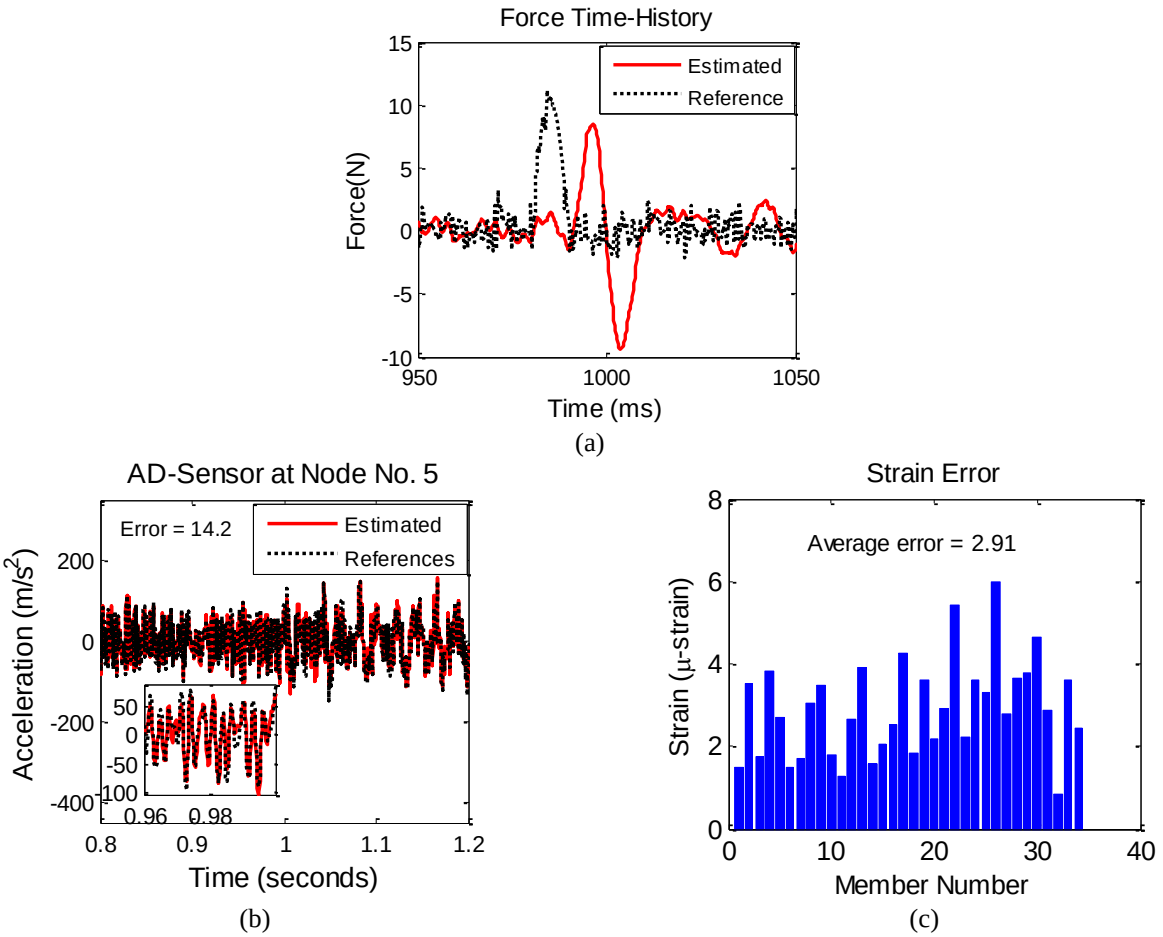

Fig. 11 Example of (a) Impact force and (b) and (c) structural response estimates with incorrect force location and assumed co-variance values for case-2

three strain gauges, as shown in Fig. 10. Four of the accelerometers are used as AD-sensors to compare the measured and estimated responses and the other three accelerometers and four strain gauges are used as SE-sensors for AKF process.

Average estimation error in the AD-sensors is calculated for all possible sensor role combinations and impact force locations. Results for one of the combinations with incorrect (initial assumption) location and assumed co-variances are given in Fig. 11. Both force and response estimations are not so good. Although accelerometers are used as AD-sensors but still error bars between actual and estimated strains are shown in Fig. 11(c), this is because these errors are meant to show the quality of structural response estimation and are not related to AD-sensor measurements.

The average error variation with the change in impact force locations for one of the sensor role combinations is shown in Fig. 12. The average error is minimum when the assumed impact force is acting at node no. 14, which is the true location of the force applied. Similar patterns are observed for all other sensor role combinations. The

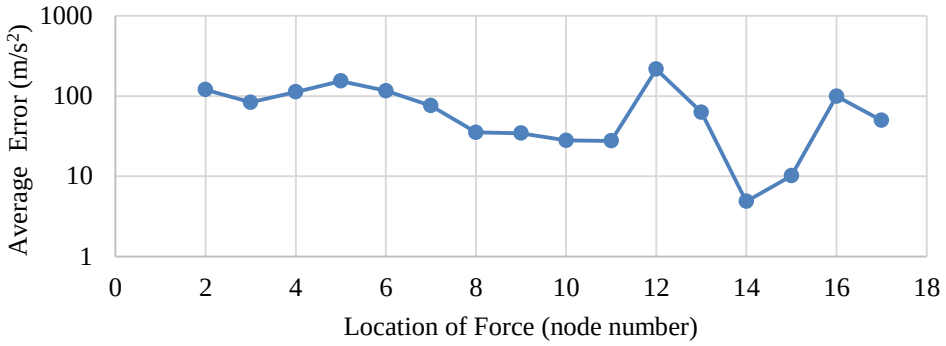

Fig. 12 Variation in average acceleration error of AD-sensors with changing force location

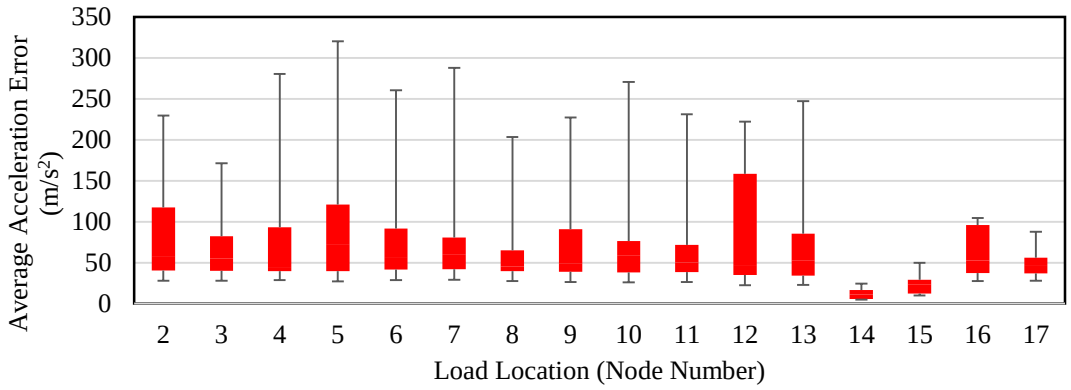

Fig. 13 Distribution of average acceleration error with change in force location for all sensor combinations

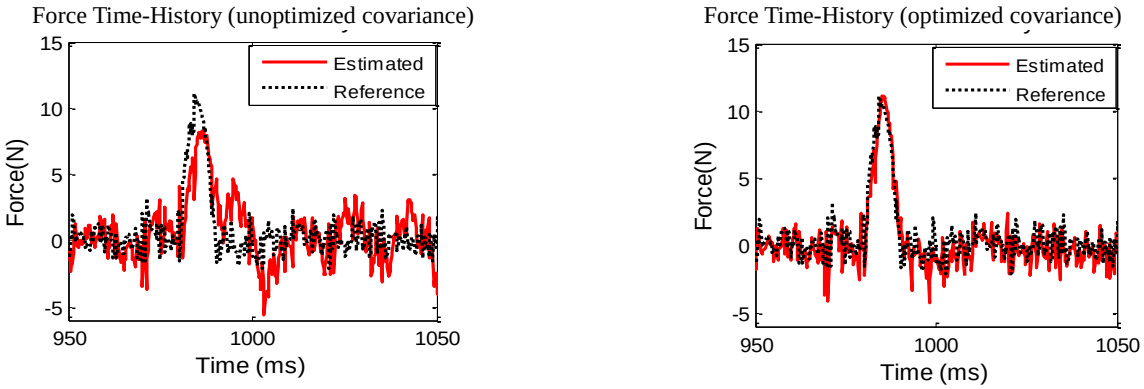

Fig. 14 Comparison of force time-history with (a) unoptimized and (b) optimized co-variance values

distribution of average error with the variation in the impact force locations is shown in Fig. 13.

As expected, the best estimation (lowest estimation error) is obtained when assumed location of the impact force is node 14, which is the true location of the force. Comparison of Figs. 5 and 13 shows that average error in AD-sensors is subjected to more variation when accelerometers are used as AD-sensors. However, the impact force location identification is still correct. Covariance matrices are optimized by minimizing the average acceleration error in AD-sensor measurements using the correct location of force. The comparison of the impact force and structural response estimations with optimized and un-optimized co-variances is presented in Figs. 14-16. Optimization of co-variances results in the more accurate estimation of both force and structural response.

The effect of relative measurement noise is considered for case-2 simulations as well and the results are presented in Fig. 17. The comparison of Figs. 15 and 16 with Fig. 17 shows that the estimation errors are slightly higher for 10% measurement noise case which indicates that the effect of 10% noise is relatively larger as compared with 1μ-strain and 1 milli-g noise levels.

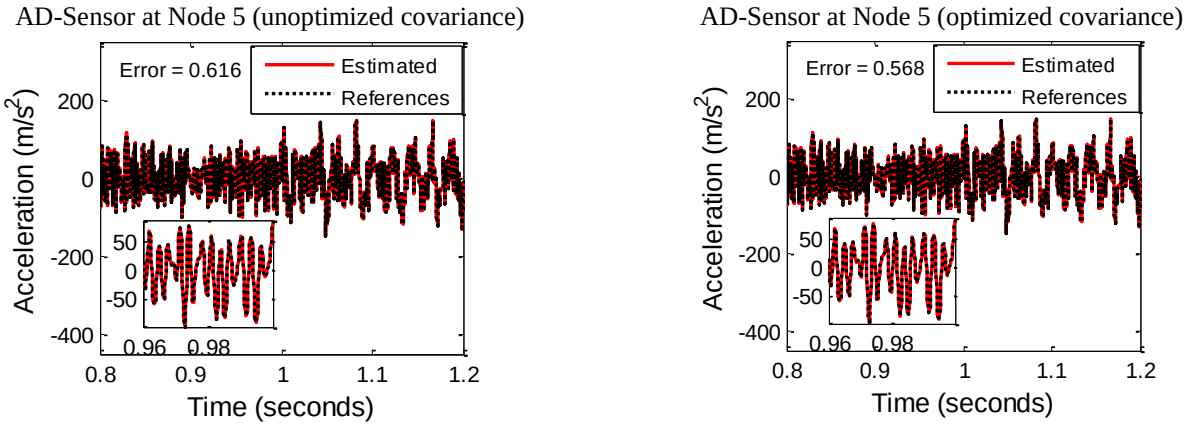

(a) (b)

Fig. 15 Comparison of estimated and measured acceleration time-history of an additional sensor for (a) unoptimized and (b) optimized co-variance values

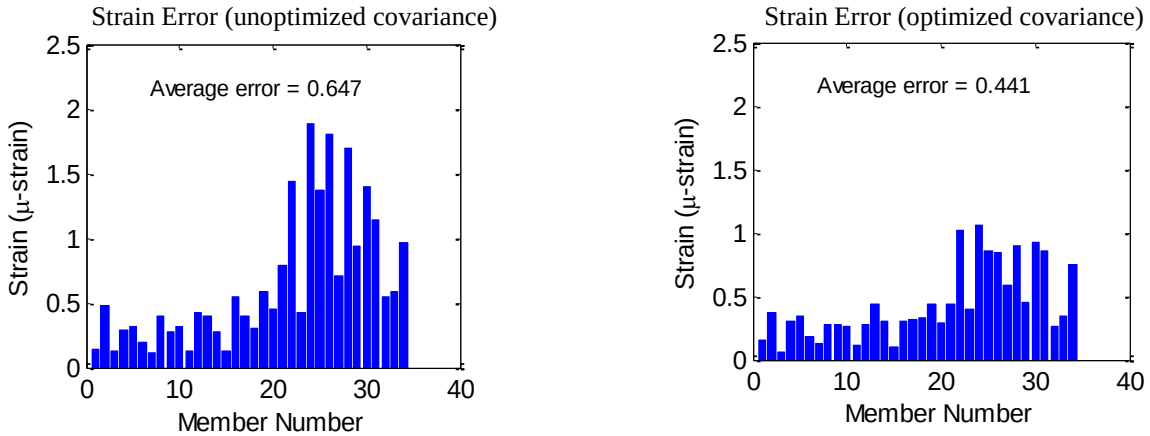

(a) (b)

Fig. 16 Comparison of member strain errors between actual and estimated strain with (a) unoptimized and (b) optimized co-variance values

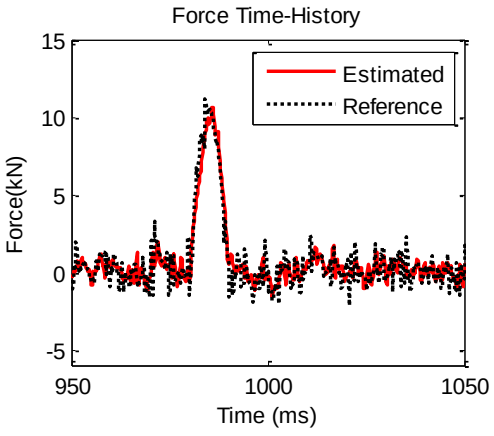

(a)

Continued-

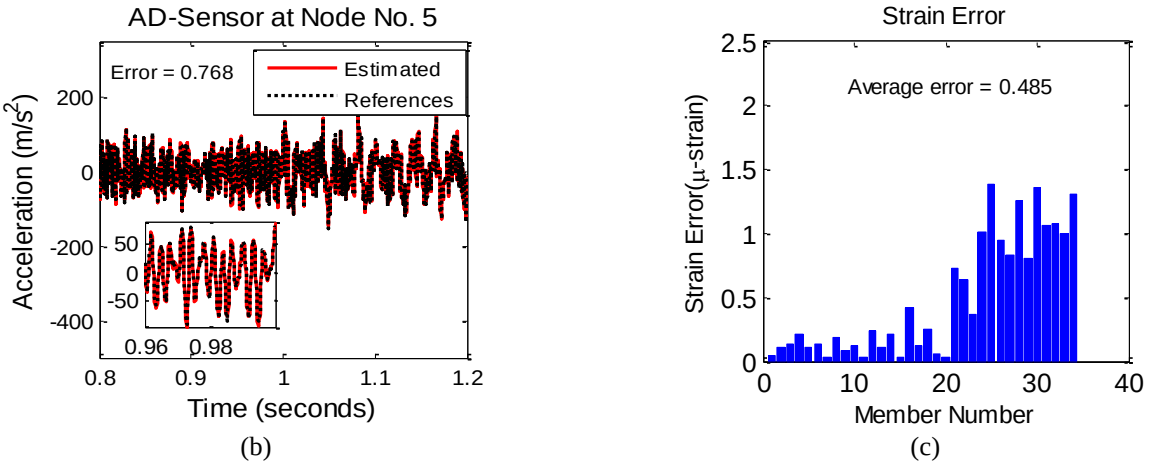

Fig. 17 (a) Impact force and (b) and (c) structural response estimates with correct force location and optimized co-variance values for case-2 considering 10% measurement noise

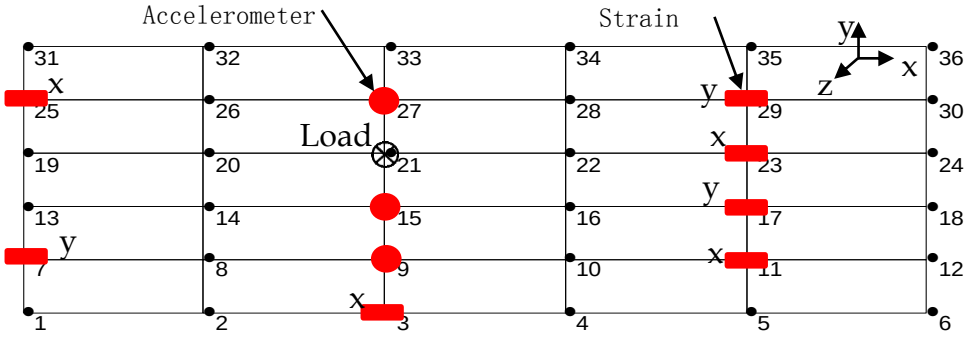

Fig. 18 Sensor arrangement for plate structure

4.2 Plate structure

Another numerical validation has been investigated using a cantilever plate model (see Fig. 18) with more number of possible impact force locations and higher number of degrees of freedom (DOF). The plate has 108 DOF which is three times more than that of the truss with 36 DOF, making it a much more complicated structure. The shorter side of the plate, from nodes 6 through 36, is fixed. From the truss structure, numerical example, performances of the proposed impact force localization method have already been validated for both cases using strain gauges or accelerometers as the AD-sensors; both cases show similar results. So, this cantilever plate numerical example will only investigate the case using strain gauges as the AD-sensors. The impact force is applied at node no. 21 in z-direction. The arrangement of the sensors on the plate is shown in the Fig. 18. Three accelerometers are used to measure z-direction accelerations. Seven strain gauges are used to measure strain responses in different directions; the orientation of strain gauges (either x or y) is labeled in the Fig. 18.

All possible thirty locations (except the fixed boundary) of the impact force have been considered for all combinations of sensors' role just like the truss structure. A comparison of actual and estimated results for an incorrect (initially assumed) location of the impact force with assumed error co-variances are shown Fig. 19. Strain gauges at nodes 3, 11, 23 and 7 are considered as AD-sensors for the example results shown in the Fig 19. The results show that the impact force estimate (Fig. 19(a)) is totally incorrect and strain estimate (Fig. 19(b)) is also quite bad with this incorrect location of the impact force. The strain estimation error bars shown in Fig. 19(c) represent strain error in x-direction (DOF 1 to 36), y-direction (DOF 37 to 72) and shear strain (DOF 73 to 108). It is evident that neither impact force nor response estimation is accurate for the incorrect force location.

The variation in average error with the change in the impact force location for one of the sensor combinations is shown in Fig. 20. The average error is minimum for node-21, which is the true location of the impact force.

The distribution of average strain error in AD-sensors for all sensor role combinations is plotted in Fig. 21. The same observation can be made as Fig. 20, the mean value of average error and its variation are the smallest for node-21 which is the true location of the impact force. It is observed that the variation for nodes 15, 27 and 9 are also relatively small for this case, because these nodes are close to the actual location of the impact force. But the mean values of the average error for these three nodes (15, 27, and 9) are higher than that of node 21, which makes our selection of the most probable impact location be still node 21.

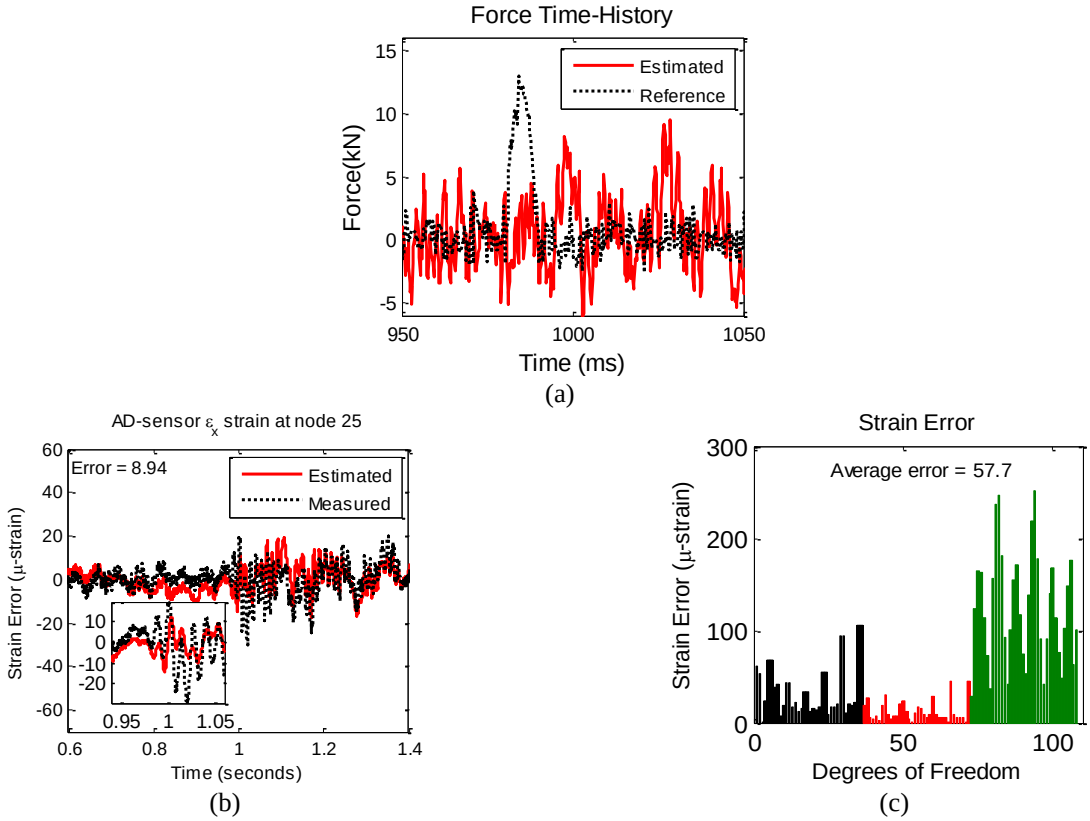

Fig. 19 Example of (a) Force and (b) and (c) Structural Response estimates with incorrect force location and assumed co-variance values for Plate

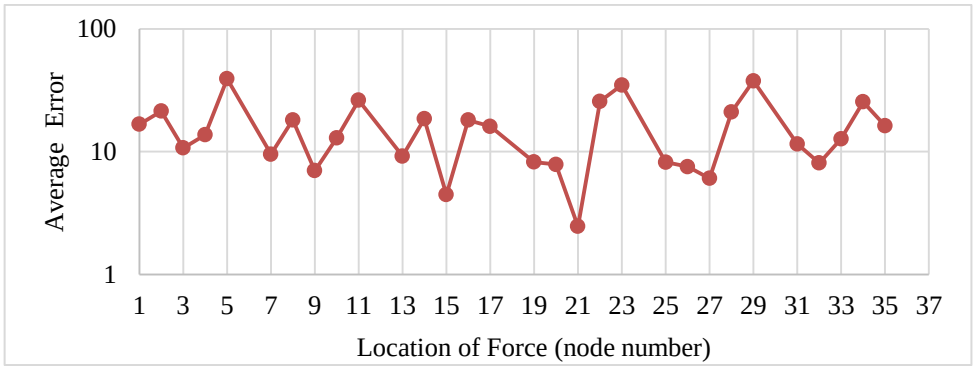

Fig. 20 Variation in average strain error of AD-sensors with changing force location for plate

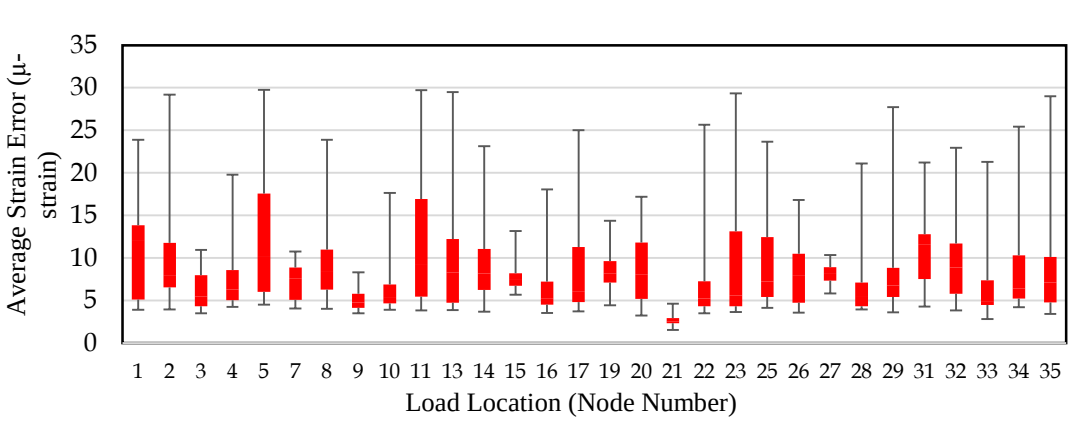

Fig. 21 Distribution of average strain error with change in force location for all sensor combinations

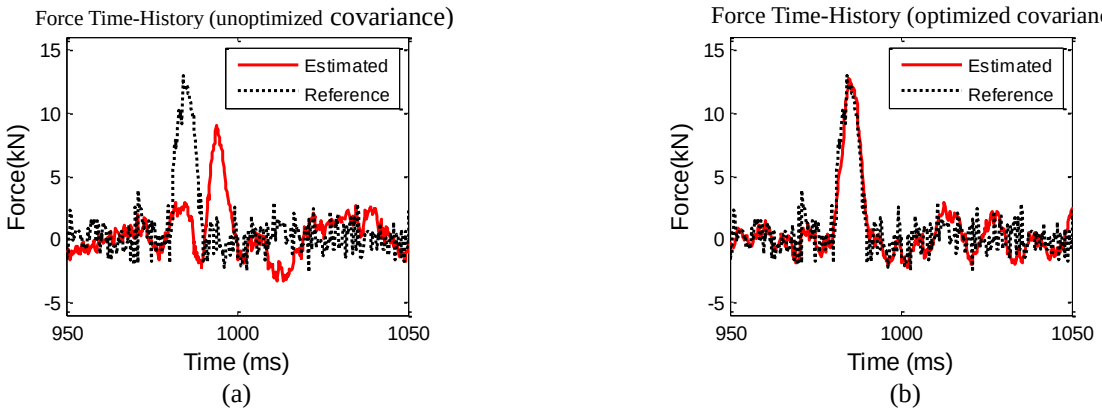

Fig. 22 Comparison of Force Time-History with (a) unoptimized and (b) optimized co-variance values

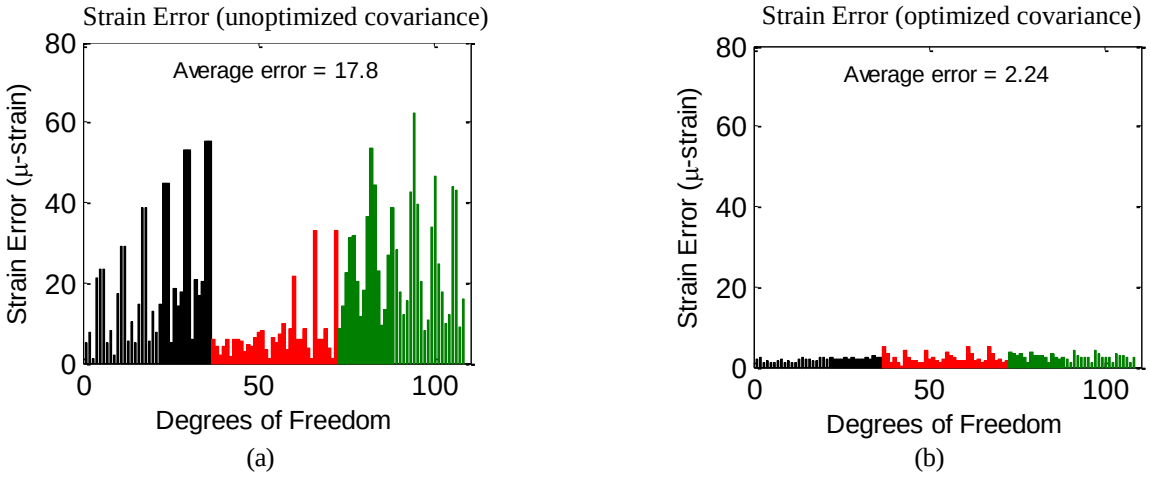

Fig. 23 Comparison of ε_x, ε_y, and γ_{xy} errors between actual and estimated strain with (a) unoptimized and (b) optimized co-variance values

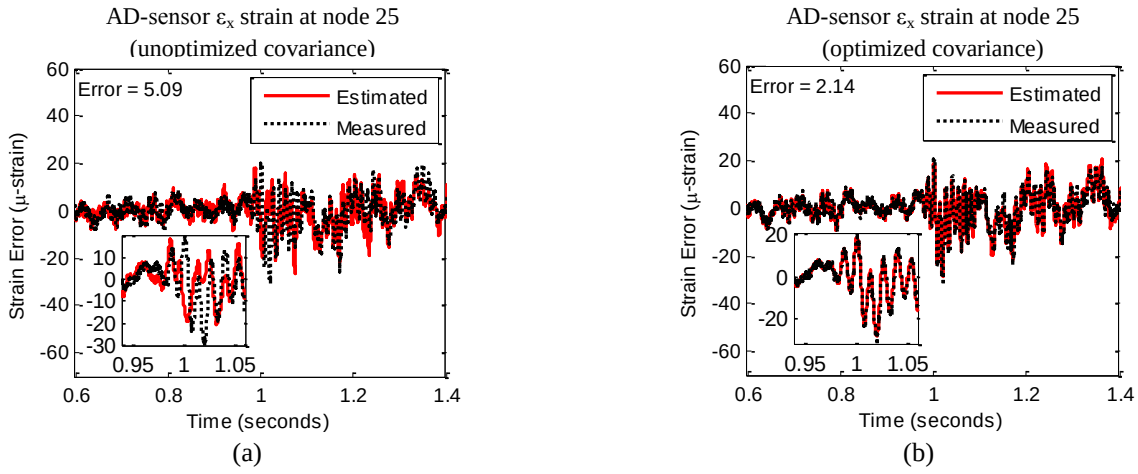

Fig. 24 Comparison of estimated and measured strain time-history of an AD-sensor for (a) unoptimized and (b) optimized co-variance values

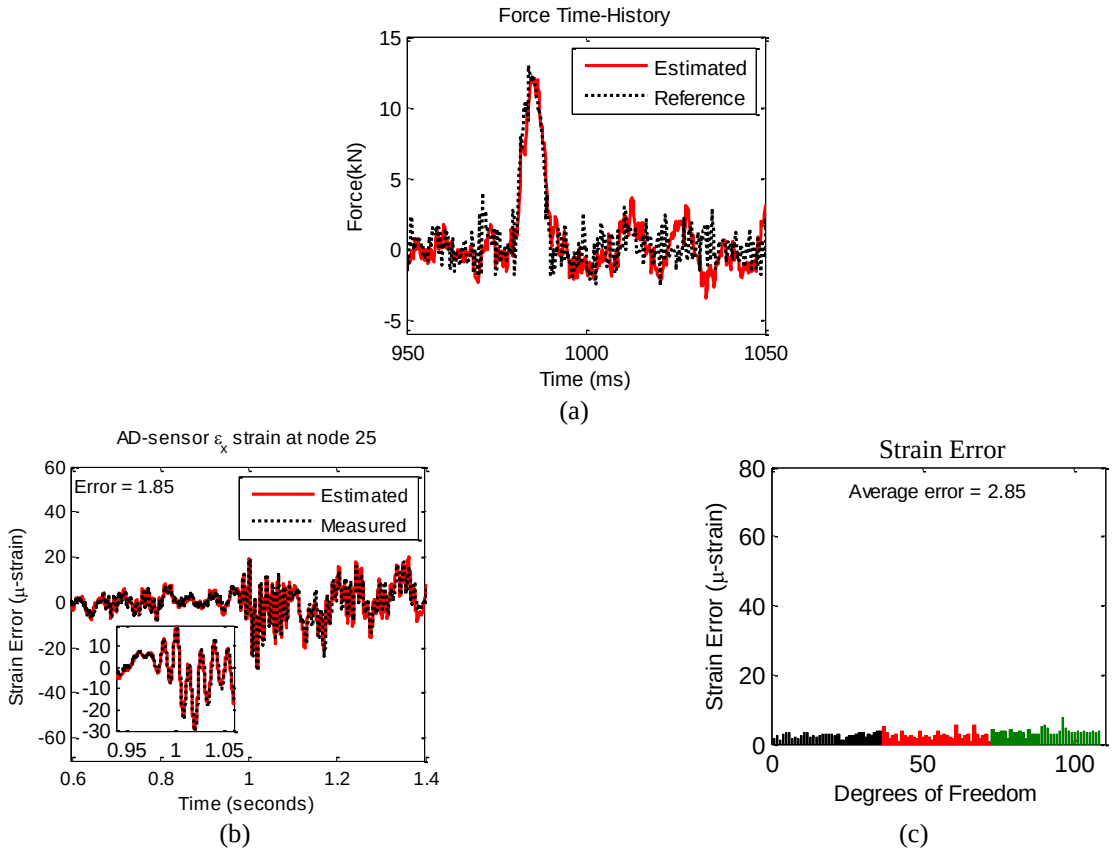

Fig. 25 (a) Impact force and structural (b) and (c) response estimates with correct force location and optimized co-variance values for Plate considering 10% measurement noise

Covariance optimization is performed for this case as well using GA after the identification of impact force location. Comparison of the impact force time-history and structural response for optimized and un-optimized co-variances is presented in Figs. 22-24, showing that more accurate results can be obtained after the optimization of the covariance values. The effect of covariance optimization is much more significant on plate response estimation (see Fig. 23) as compared with the truss response estimation (Figs. 8 and 16), this may be either because of relative poor initial guess of covariance values or more complicated structural behavior of plate.

The results of 10% measurement noise case for the plate are shown in Fig. 25 which shows that the both the impact force and structural response can be estimated with comparable quality as that of absolute noise case.

5. Conclusions

This paper presents a novel approach for the complete identification (location and time history) of impact force using multi-metric observations. The proposed method utilizes AKF, which is a variant of conventional KF, to locate the impact force and then GA is applied to optimize the co-variances. Finally, accurate identification of applied impact force and structural response is achieved by using optimized co-variances in AKF.

Two numerical examples, a simply supported truss and a cantilever plate are used to validate the proposed method. Two types of sensor measurements i.e., strain, and acceleration are used for impact force identification. Results of both the examples show that the proposed method can effectively identify the location, duration and peak of the impact force. Results also show that both strain and acceleration measurements can correctly identify the impact force. It was also observed that the impact force is more sensitive to the co-variance values as compared with the structural response. Good performance of the proposed method establishes its potential to be applied for impact force identification in real life structures. Of note the proposed method can also be extended to identify the impact load induced by moving traffic or train on bridges. Nevertheless, a possible future study could be the experimental validation of this method.

Acknowledgements

The authors would like to thank University of Engineering and Technology, Lahore, Pakistan for supporting this research under Faculty Development Program.

References

Bishop, G. and Greg, W. (2001), "An introduction to the Kalman filter", *Proc.of SIGGRAPH, Course*, 8, North Carolina, USA.

Buth, C.E., Williams, W.F., Brackin, M S., Lord, D., Geedipally, S. R. and Abu-Odeh, A.Y. (2010), "Analysis of large truck collisions with bridge piers: phase 1. Report of guidelines for designing bridge piers and abutments for vehicle collisions", *Texas: Texas Transportation Institute*.

Busby, H.R. and Trujillo, D.M. (1997), "Optimal regularization of an inverse dynamics problem", *Comput. Struct.*, **63**(2), 243-248.

Choi, K.Y. and Chang, F.K. (1996), "Identification of impact force and location using distributed sensors", *AIAA J.*, **34(**1), 136-142.

Coverley, P.T. and Staszewski, W.J. (2003), "Impact damage location in composite structures using optimized sensor triangulation procedure", *Smart Mater. Struct.*, **12**(5), 795-803.

Golub, G.H. and Von Matt, U. (1997), "Generalized cross-validation for large-scale problems", *J. Comput. Graph. Stat.*, **6**(1), 1-34.

Guillaume, Patrick, et al. (2002), "An inverse method for the identification of localized excitation sources", *Proceedings of the IMAC*, Los Angeles, USA, February

Hansen, P.C. (1992), "Analysis of discrete ill-posed problems by means of the L-curve", *SIAM Review*, **34**(4), 561-580.

Inoue, H., Harrigan, J.J. and Reid, S.R. (2001), "Review of inverse analysis for indirect measurement of impact force", *Appl. Mech. Rev.*, **54(**6), 503-524.

Jacquelin, E., Bennani, A. and Hamelin, P. (2003), "Force reconstruction: analysis and regularization of a deconvolution problem", *J. Sound Vib.*, **265**(1), 81-107.

Juang, J.N. and Phan, M.Q. (2001), *Identification and Control of Mechanical Systems*, Cambridge University Press, Cambridge, England

Khodabandeloo, B. and Jo, H.K. (2015), "Broadband dynamic load identification using augmented Kalman filter", Joint Conference AESE/ANCRiSST, Urbana, Illinois, USA, August.

Kijewski-Correa, T., Su, S., Abittan, E. and Antsaklis, P.J. (2006), "On the use of heterogeneous, wireless sensor networks for damage assessment in bridges under unknown excitations", *Proceedings of the 4th World Conference on Structural Control and Monitoring*, San Diego, California, USA, July

LeClerc, J.R. *et al.* (2007), "Impact detection in an aircraft composite panel - A neural-network approach", *J. Sound Vib.*, **299**(3), 672-682.

Liu, J.J. *et al.* (2000), "Input force estimation of a cantilever plate by using a system identification technique", *Comput. Method. Appl. M.*, **190**(11), 1309-1322.

Lourens, E. *et al*. (2012), "An augmented Kalman filter for force identification in structural dynamics", *Mech. Syst. Signal Pr.*, **27**, 446-460.

Ma, C.K. and Lin, D.C. (2000), "Input forces estimation of a cantilever beam", *Inverse Probl. Eng.*, **8**(6), 511-528.

Ma, C.K. *et al.* (1998), "A study of an inverse method for the estimation of impulsive loads", *Int. J. Syst. Sci.*, **29**(6), 663-672.

Mahzan, S., Staszewski, W.J. and Worden, K. (2010), "Experimental studies on impact damage location in composite aerospace structures using genetic algorithms and neural networks", *Smart Struct. Syst.*, **6**(2), 147-165.

Mahzan, S. (2007), "Impact location in composite structures using advanced signal processing procedures", *Ph.D.* Dissertation, University of Sheffield, South Yorkshire, England.

Meo, M. *et al.* (2005), "Impact identification on a sandwich plate from wave propagation responses", *Compos. Struct.*, **71**(3), 302-306.

Naets, F., Cuadrado, J. and Desmet, W. (2015), "Stable force identification in structural dynamics using Kalman filtering and dummy-measurements", *Mech. Syst. Signal Pr.*, **50**, 235-248

Papadimitriou, C., Fritzen, C.P., Kraemer, P. and Ntotsios, E. (2011), "Fatigue predictions in entire body of metallic structures from a limited number of vibration sensors using Kalman filtering", *Struct. Control Health Monit.*, **18**(5), 554-573.

Qiu, L. and Yuan, S. (2011), "A phase synthesis time reversal impact imaging method for on-line composite structure monitoring", *Smart Struct. Syst.*, **8**(3), 303-320

Seydel, R. and Chang, F.K. (2001), "Impact identification of stiffened composite panels: I. System development", *Smart Mater. Struct.*, **10**(2), 354-369.

Sharif-Khodaei, Z., Ghajari, M. and Aliabadi, M.H. (2012), "Determination of impact location on composite stiffened panels", *Smart Mater. Struct.*, **21(**10), 105026(14pp)

Sim, S.H., Spencer Jr., BF. and Nagayama, T. (2011), "Multi-metric sensing for structural damage detection", *J. Eng. Mech. - ASCE*, **137**(1), 22-30

Staszewski, W.J., Mahzan, S. and Traynor, R. (2009), "Health monitoring of aerospace composite structures–Active and passive approach", *Compos. Sci. Technol.*, **69**(11), 1678-1685.

Sung, D.U. *et al.* (2000), "Impact monitoring of smart composite laminates using neural network and wavelet analysis", *J. Intel. Mat. Syst. Struct.*, **11**(3), 180-190.

Worden, K. and Staszewski, W.J. (2000), "Impact location and quantification on a composite panel using neural networks and a genetic algorithm", *Strain*, **36**(2), 61-68.

Yan, G. and Zhou, L. (2009), "Impact load identification of composite structure using genetic algorithms", *J. Sound Vib.*, **319**(3), 869-884.

Yan, G., Sun, H. and Büyüköztürk, O. (2017), "Impact load identification for composite structures using Bayesian regularization and unscented Kalman filter", *Struct. Control Health Monit.*, **24**(5)

Zhang, X., Liang, D., Zeng, J. and Lu, J. (2014), "SVR model reconstruction for the reliability of FBG sensor network based on the CFRP impact monitoring", *Smart Struct. Syst.*, **14**(2), 145-158

HJ